

Indistinguishability of remote quantum dot-cavity single-photon sources

Mathias Pont,^{1,2,*} Stephen C. Wein,² Ilse Maillette de Buy Wenniger,^{1,3} Valentin Guichard,¹
Nathan Coste,^{1,4} Abdelmounaim Harouri,¹ Aristide Lemaître,¹ Isabelle Sagnes,¹ Loïc
Lanco,^{1,5} Nadia Belabas,¹ Niccolo Somaschi,² Sarah E. Thomas,^{1,3} and Pascale Senellart^{1,†}

¹*Université Paris-Saclay, Centre de Nanosciences et de Nanotechnologies,*

CNRS, 10 Boulevard Thomas Gobert, 91120, Palaiseau, France

²*Quandela SAS, 7 Rue Léonard de Vinci, 91300 Massy, France*

³*Department of Physics, Imperial College London, London, UK*

⁴*School of Mathematical and Physical Sciences, University of Technology Sydney, Ultimo, New South Wales 2007, Australia*

⁵*Université Paris Cité, Centre de Nanosciences et de Nanotechnologies,*

CNRS, 10 Boulevard Thomas Gobert, 91120, Palaiseau, France

(Dated: December 23, 2024)

Generating identical photons from remote emitter-based bright single-photon sources is an important step for scaling up optical quantum technologies. Here, we study the Hong-Ou-Mandel interference of photons emitted from remote sources based on semiconductor quantum dots. We make use of a deterministic fabrication technique to position the quantum dots in a spectrally resonant micropillar cavity and fine tune their operation wavelength electrically. Doing so, we can match four pairs of sources between five distinct sources, study them under various excitation schemes and measure their degree of indistinguishability. We demonstrate remote indistinguishability between $44 \pm 1\%$ and $69 \pm 1\%$ depending on the pair of sources and excitation conditions, record values for quantum dots in cavities. The relative contribution of pure dephasing and spectral diffusion is then analysed, revealing that the remaining distinguishability is mostly due to low frequency noise.

I. INTRODUCTION

The number of qubits involved in photon-based quantum information processing protocols is largely determined by the efficiency of indistinguishable single-photon sources. Two main single-photon source technologies are now routinely exploited. Sources based on photon pair generation in non-linear media and photon heralding allowed impressive progresses [1–3]. Due to the probabilistic generation process, a massive integration of sources and detectors is required to scale up [4]. More recently, single-photon sources (SPS) based on semiconductor quantum dots (QDs) have been shown to generate on-demand indistinguishable single-photons, at high efficiency when inserted in optical cavities [5–8]. Their compatibility with low-loss integrated optical circuits, and high-efficiency single-photon detectors have made them important contenders for intermediate scale quantum computation [9–12]. To generate multi-photon states with QD-based sources, the current approach has been to use active demultiplexing of a temporal stream of identical photons generated by one bright source [9, 10, 12–16]. In parallel to increasing a single source efficiency, further scaling will eventually require making use of many identical SPS [17].

The generation of indistinguishable photons from remote QD based single-photon sources has motivated many works in the past fifteen years [18–34]. The first requirement for high remote source indistinguishability

is the ability to tune the two sources to the same wavelength within the emission linewidth. The two photonic wavepackets should also present the same temporal profile, a challenging requirement when the QDs are inserted into an optical cavity for high photon collection: both emitters should then undergo similar acceleration of spontaneous emission. Last but not least, each quantum emitter should emit infinite trains of identical photons. This requires that the QD does not suffer from decoherence during the emission process (no pure dephasing) nor on a long time scale (no spectral diffusion). An important milestone has recently been achieved with the demonstration of a remote two-photon indistinguishability of $(93.0 \pm 0.8)\%$ with GaAs QDs in a bulk medium [31], albeit at low collection efficiency. Very few works have studied the indistinguishability of remote QD in cavities - ensuring high collection efficiency, with remote indistinguishability at best in the 40 % range [23].

Here, we report on the measurement of remote two-photon indistinguishability from multiple QD-cavity based single-photon sources. We harness a deterministic fabrication technique based on optical in-situ lithography [35] to fabricate two samples with multiple QD-micropillar sources. Selection of QDs with similar as-grown emission wavelength combined with fine electrical spectral tuning allow us to identify five sources distributed in four pairs of spectrally matched sources presenting a classical temporal overlap between $(98.4 \pm 0.1)\%$ and $(99.6 \pm 0.1)\%$. We study the quantum interference of photons emitted by these various remote sources under either resonant or phonon-assisted excitation schemes. All pairs reach record values of remote two-photon indistinguishability for QD in cavities up to $69 \pm 1\%$. Time delay dependent analysis of the indistinguishability of suc-

* mathias.pont@quandela.com

† pascale.senellart-mardon@cnrs.fr

cessively emitted photons from the most identical sources allow us to identify the contribution of pure dephasing and spectral wandering to the remaining distinguishability.

II. SINGLE PHOTON SOURCE DEVICES

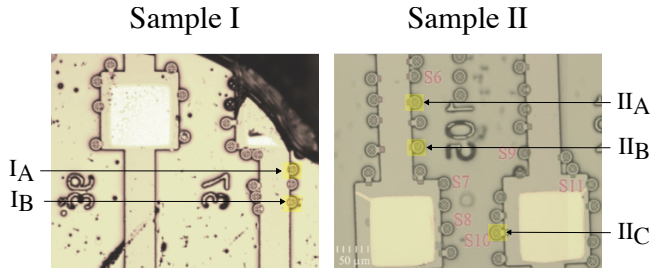


FIG. 1: Optical microscope image of the two samples under study. We indicate on each the sources that can be brought to resonance with another source of the other sample. The four pairs are $\{I_A, II_A\}$, $\{I_A, II_B\}$, $\{I_B, II_B\}$ and $\{I_B, II_C\}$.

We study two samples labelled I and II, shown in Fig. 1, fabricated from the same molecular-beam-epitaxy grown planar cavity wafer consisting of isolated InGaAs QDs embedded in a λ -cavity with 14 (28) GaAs/AlAs Bragg pairs in the top (bottom) mirror. A 20 nm-thick $\text{Ga}_{0.1}\text{Al}_{0.9}\text{As}$ barrier, positioned 10 nm above the QD layer, is used to increase the hole capture time inside the QD. The *in-situ* lithography technique [6, 35, 36] was used to deterministically position a single QD within 50 nm of the center of a connected pillar cavity. The Purcell effect in the weak coupling regime allows for a large fraction of the single-photon emission to be funnelled into the pillar cavity mode. The *in-situ* lithography process allows the adjustment of the pillar cavity diameter to ensure the spectral resonance between the QD and the cavity lines is better than 0.5 nm [35].

Each sample embeds a vertical p-i-n diode structure and the pillars are electrically contacted to operate in the reverse-bias regime. This enables different occupation states for the QD ground state depending on the applied voltage. In the following, we study both neutral and charged QD sources. The electrical bias also allows us to fine tune the QD-cavity detuning within a 0.3-0.5 nm range depending on the source [36]. The performances of the samples studied here were previously benchmarked in terms of source brightness, single-photon purity and indistinguishability as reported in Ollivier et al. [37]. An average indistinguishability of $(90.6 \pm 2.8)\%$, single-photon purity of $(95.4 \pm 1.5)\%$ were reported over 5 samples, including samples I and II. The average first lens brightness \mathcal{B} , i.e. the probability to get a photon per excitation pulse at the output of the micropillar device, was found to be $(13.6 \pm 4.4)\%$.

The mean operation wavelength yielding optimal performances of all the sources across samples I and II was shown to be 924.7 nm with a standard deviation 0.5 nm. Among the single-photon sources of each samples, we identify several pairs of sources that can be tuned to the same emission energy. Fig. 1 shows optical microscope images of the two samples and highlight the 5 sources, two on sample I (I_A and I_B), three on sample II (II_A , II_B , II_C) that can be spectrally matched two by two to form 4 pairs as shown later on.

We explore the interference of photons emitted by remote sources using two excitation schemes: resonant excitation and longitudinal acoustic (LA) phonon assisted excitation. Both excitation techniques have been shown to lead to high indistinguishability for photons successively emitted by the same source [38]. Resonant excitation results in a near unity occupation probability of the QD excited state that allowed record source brightness [7, 39]. However, it requires to collect the single photons in crossed polarisation with respect to the excitation laser polarisation [6, 7, 21] which remove useful spin information for graph state generation. LA-phonon-assisted excitation allows to spectrally filter the laser and to generate polarization-entangled multi-photon states through spin-photon entanglement [40], at the expense of a slightly reduced excited state occupation probability. Both schemes lead to different temporal profiles, which influences the remote source interference.

III. WAVELENGTH AND TEMPORAL OVERLAP

High indistinguishability for single photons generated by two quantum emitter sources first requires that both sources are spectrally matched and present the same emission profile. For two remote dipoles labelled i and j showing mono-exponential decay times $T_{1,i}$ and $T_{1,j}$, in the absence of any decoherence process, the two-photon mean wavepacket overlap is given by [23]

$$M_{i,j} = \frac{4\gamma_i\gamma_j}{(\gamma_i + \gamma_j)^2 + \Delta_{i,j}^2}, \quad (1)$$

with the emission rate defined as $\gamma_i = 1/T_{1,i}$ and $\gamma_j = 1/T_{1,j}$ and $\Delta_{i,j} = \omega_i - \omega_j$ the frequency difference between the two sources. When the two sources are spectrally matched ($\Delta_{i,j} = 0$), the upper limit for remote indistinguishability is then the classical temporal overlap $s_{i,j} = 4\gamma_i\gamma_j/(\gamma_i + \gamma_j)^2$ which reaches unity for $\gamma_i = \gamma_j$. For emitters in cavities, the lifetime depends on the detuning between the emission energy of the QD and the energy of the cavity mode. Moreover, the highest photon collection efficiency for each source requires each QD transition to be tuned to their respective cavity resonance. Hence, a strong requirement for optimal temporal and spectral overlap is to fabricate devices with strongly overlapping cavity resonances.

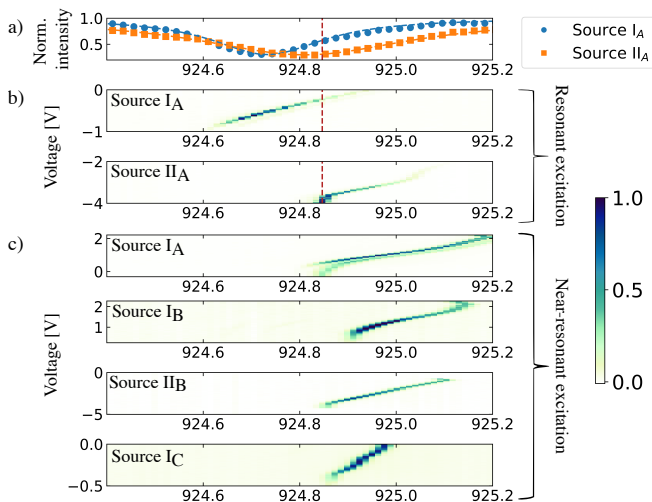


FIG. 2: (a) Reflectivity spectra of source I_A and II_A measured using a broad-band LED source in a polarisation resolved reflectivity setup. (b-c) Emission wavelength of each source as a function of the applied voltage bias under (b) resonant excitation and (c) LA-phonon-assisted excitation. As shown in (a-b) with the matching pair I_A and II_A , by tuning two sources into resonance (indicated by the dotted red vertical line) we move away from the exact individual resonances of the microcavities described by Lorentzian fits for both source I_A (blue circles) and source II_A (orange squares) shown in panel (a).

Fig. 2a shows the reflectivity spectra of two devices (I_A and II_A), one on each sample, measured using a broadband LED source in a polarisation resolved reflectivity setup. The measurement evidences substantial overlap of the two cavity modes and the lorentzian cavity fit yields $Q_{I_A}=2900$ ($Q_{II_A}=1700$) at $x_{c,I_A}=924.734$ nm ($x_{c,II_A}=924.817$ nm) for source I_A (II_A) where the quality factor Q_i is the ratio of the central frequency $x_{c,i}$ and the full width at half-maximum of the fundamental mode of the micro-cavity of source i .

Fig. 2b-c show the QD emission energy of each source tuned by application of a bias. The current flowing through the diodes are measured to be below pA. We use both for resonant excitation (b) and LA-phonon-assisted excitation (c). The intensity maps allow to define the voltage range where each source can be put in resonance with another one. We identify 4 pairs of sources that can be tuned to respective resonance: ($\{I_A, II_A\}$, $\{I_A, II_B\}$, $\{I_A, II_C\}$ and $\{I_B, II_B\}$). For most pairs, under LA-phonon-assisted excitation, we can set a voltage where both sources are closed to mutual QD energy resonance while being close to their maximal emission intensity. For resonant excitation, the same ~ 15 ps laser pulse is used to excite both QDs so that the scan does not reflect the full tuning range of the source but is constrained by the chosen laser energy. We note moreover that the use of much lower pump power in resonance excitation (below 1 nW) compared to LA-phonon-assisted excita-

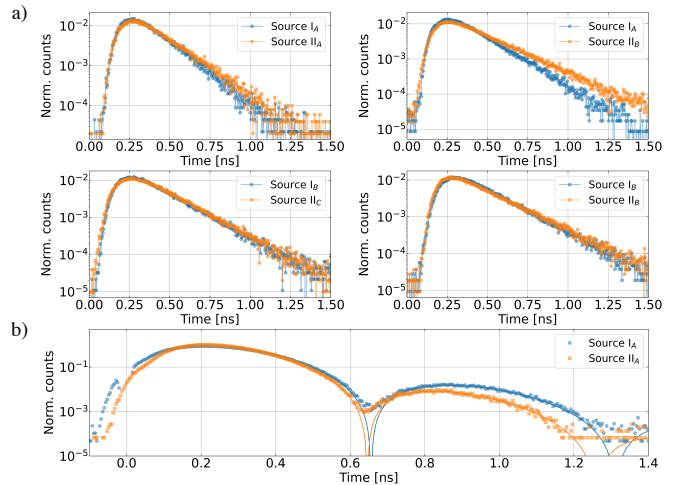


FIG. 3: Overlapped time evolution of the PL emission (a) under LA-phonon-assisted excitation of source $\{I_A, II_A\}$, $\{I_A, II_B\}$, $\{I_B, II_B\}$ and $\{I_B, II_C\}$, and (b) resonant PL emission for source $\{I_A, II_A\}$. The integrated counts per time bin have been normalised by the integrated area of the full temporal profile.

tion (few μ W), displaces the bias tuning range of interest. Fig. 2b presents a scan under resonant excitation for sources I_A and II_A . We observe that while I_A is tunable over a wide energy range, QD II_A can not be tuned below 924.847 nm (Fig. 2b). In this case, we tune the emission energy of I_A to the wavelength where II_A is the brightest (indicated by the dotted red vertical line). The detuning between source I_A (source II_A) and its microcavity is thus $\Delta_{I_A}=113$ pm ($\Delta_{II_A}=30$ pm). This mutual resonance point leads to a decrease of the brightness for I_A from $\mathcal{B}_{I_A} \sim 15.4\%$ to $\mathcal{B}_{I_A} \sim 12.4\%$, while the brightness of II_A is $\mathcal{B}_{II_A} \sim 18.5\%$.

We now turn to the temporal profiles of emission of the sources at their mutual resonance. Here, the use of phonon-assisted excitation or resonant excitation alters significantly the temporal emission profiles. The simple situation described by Eq. (1) correctly describes the case of phonon-assisted excitation for which a mono-exponential decay emission profile can always be obtained independently of the charge state of the QD. A charged QD (trion) corresponds to a four-level system for which both the ground and the excited states are degenerate. Such state structure can effectively be described as two-level system with a single time constant for the emission hence mono-exponential decay. Conversely, a neutral QD is a three-level system composed of a single ground state and two non-degenerate linearly polarised excited states. Using LA-phonon-assisted excitation, one can align the linear polarisation of the excitation along one of the excitonic dipoles reducing the system to an effective two-level system [38], hence again to a monoexponentially decaying emission. We can thus use this excitation scheme to obtain a similar temporal profiles between neutral and charged QD sources. We

find four different pairs of sources on samples I and II, that can be tuned in resonance, and have a very similar time evolution profiles with typical decay time $T_{1,i}$ within 128-240 ps range as shown in Fig. 3a. We deduce the corresponding classical temporal overlap $s_{i,j}$ which ranges from $(98.4 \pm 0.1)\%$ to $(99.6 \pm 0.1)\%$.

Under strictly resonant excitation, achieving such high temporal overlap for neutral QD sources is more demanding. This is illustrated now using sources I_A and II_A that embed neutral QDs with excited state composed of two non-degenerate states [41] labelled $|X\rangle$ and $|Y\rangle$ with energy splitting Δ_{FSS} . For a QD in a cavity under resonant excitation, the laser light polarisation is set along the $|V\rangle$ axis of the micropillar cavity in order to suppress any rotation of the laser polarisation by the cavity birefringence [37]. $|V\rangle$ is not parallel to the axis of the QD dipoles $|X\rangle$, one thus creates a superposition of the QD dipoles $|X\rangle$ and $|Y\rangle$, and observe a beating between those two excited states. Fig. 3b shows the time evolution of each source measured along the $|H\rangle$ axis of their respective microcavities.

To describe such situation that cannot be accounted within Eq. (1), we introduce the generalised classical overlap:

$$s_{i,j} = \left[\int f_i(t)f_j(t)dt \right]^2, \quad (2)$$

where $f_i(t) \propto \sqrt{\langle \hat{a}_i^\dagger(t)\hat{a}_i(t) \rangle}$ is the magnitude of the temporal amplitude of the emitted single-photon pulse normalised to $\int f_i^2(t)dt = 1$. Importantly, this classical overlap bounds the mean wavepacket overlap (see Supporting Information). We fit the measured temporal decay with

$$|\langle H|\Psi(t)\rangle|^2 = \sin^2\left(\frac{\Delta_{FSS}}{2\hbar}t\right) \sin^2(2\theta) e^{-\frac{t}{T_{1,X}}} \quad (3)$$

where θ is the angle between the optical polarization axis $|H\rangle$ and the dipole orientation of the exciton eigenstate $|X\rangle$. We find the parameters $T_{1,I_A} = (162 \pm 1)$ ps, $\Delta_{FSS,I_A} = (6.3 \pm 0.1)$ μ eV, $T_{1,II_A} = (128 \pm 1)$ ps and $\Delta_{FSS,II_A} = (6.7 \pm 0.1)$ μ eV. To compute the temporal overlap we use the measured temporal decay and obtain a value as high as $s_{I_A,II_A} = (98.6 \pm 0.1)\%$ despite the slight discrepancy in fine structure splitting. It is worth noting that such high temporal overlap from natural QDs under resonant excitation is more of a lucky coincidence, since not only do they need to have similar excitonic energy splitting but also similar angles between the polarisation of the QD dipoles and the cavity axes.

IV. REMOTE SOURCE INDISTINGUISHABILITY

We now study the quantum interference of each pair (i, j) of sources. Fig. 4a-b present the general scheme for the experimental setup. Both sources are placed in

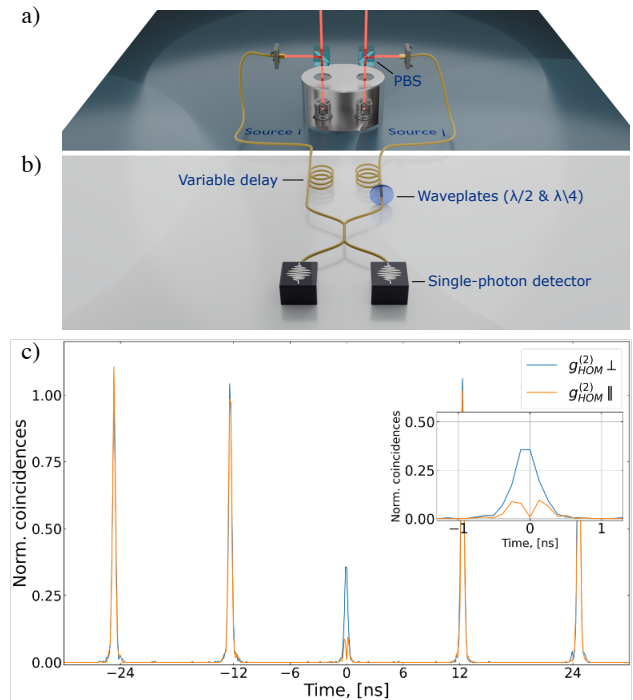


FIG. 4: (a) Scheme of the experimental setup used to measure the indistinguishability of photons emitted by two remote SPS (see text) (b) Hong-Ou-Mandel (HOM) interferometer for two-photon interference from remote emitters. (c) Example of correlation measurement acquired for sources I_A and II_A under resonant excitation using parallel (\parallel) and perpendicular (\perp) polarisation. The measurement gives a HOM visibility of $V_{TPI} = (69 \pm 1)\%$.

the same closed cycle cryostat operating at ~ 5 K on two piezo stages. A common pulsed excitation laser with a repetition rate of 82 MHz and pulse duration of ~ 10 ps is used to excite both sources. Each source is electrically tuned using two voltage controllers to set V_i and V_j . The single-photon stream from each source is sent into a fibered Hong-Ou-Mandel interferometer. A fiber delay and a free-space micrometer linear stage are used to ensure that both photons arrive simultaneously at the input of a fibered 50:50 beam-splitter (BS). Fig. 4b shows a schematic for the HOM interference where using a set of waveplates we can either set the polarisation of the photons to be parallel (\parallel) or orthogonal (\perp). We measure correlations at the output of the beam splitter using high resolution (~ 10 ps) superconducting nanowire single-photon detectors and a low time-jitter correlator (~ 12 ps). When both photons are co-polarised (\parallel), they interfere at the beam-splitter and we observe a strong antibunching, i.e. a reduction of coincidences at zero time delay. Because the sources under study can show residual blinking, the antibunching peak at zero is normalised with the central peak of the non-interfering histogram when their polarisation in orthogonal (\perp) [25, 27]. The interference-fringe visibility is thus defined by

Pair N ^o	Source label	Charge state	Excitation	$T_{1,i}$ (ps)	$s_{i,j}$	V_{TPI}
1	I _A	X	Res.	162±7	0.986±0.001	0.69±0.01
	II _A	X		128±3		
1	I _A	X	LA	158±12	0.992±0.001	0.463±0.001
	II _A	X		172±4		
2	I _A	X	LA	145±10	0.984±0.001	0.50±0.01
	II _B	CX		195±10		
3	I _A	X	LA	174±10	0.996±0.001	0.44±0.01
	II _C	CX		219±10		
4	I _B	CX	LA	240±10	0.995±0.001	0.59±0.01
	II _B	CX		212±10		

TABLE I: Remote two-photon indistinguishability V_{TPI} of 4 matching pairs of sources depending on their charge state (neutral QD – X, charged QD – CX), the excitation scheme (resonant excitation – Res., LA-phonon-assisted excitation – LA), the lifetime $T_{1,i}$ of the excited state, and the generalised classical overlap, $s_{i,j}$. All values are obtained with the additional etalon spectral filter.

$$V_{TPI} = 1 - \frac{A_{\parallel}}{A_{\perp}}, \quad (4)$$

where A_{\parallel} and A_{\perp} is the integrated zero-delay peak in presence of quantum interference and without quantum interference, respectively. The interference of sources I_A and II_A under resonant excitation shows an interference visibility of $V_{TPI} = (54.8 \pm 1)\%$. Such value already constitutes a record value for remote single photon sources based on QDs in cavities [23]. This value is further increased to $V_{TPI} = (69 \pm 1)\%$ (see Fig. 4c) when the single-photon are filtered with an 8 pm air-spaced etalon at the cost for reducing the effective source brightness by roughly 50%. This spectral filtering that does not influence the temporal decay of the state (see Supporting Information), as the width of the filter is larger than the radiative linewidth of the QDs. The increased visibility thus indicates some influence of either phonon-sideband emission or spectral wandering i.e. low frequency charge noise. The same pair of sources shows a reduced remote interference visibility of $V_{TPI} = (46.3 \pm 0.1)\%$ when operated in the phonon-assisted excitation regime.

Tab. I presents the experimental data gathered on all the matching pairs on both samples, including excitation scheme, temporal decay time, classical temporal overlap, and remote two-photon indistinguishability. All values reported are measured with the additional (8 pm) spectral filter where very low second-order correlation function $g^{(2)}(0)$ between 0.3% and 1% are reached. The remote two-photon indistinguishability ranges from 44% to 69% - with an average value of $(54 \pm 9)\%$, setting new records for QD sources in cavities.

Source label	Excitation	M_i	$\sqrt{M_i M_j}$
I _A	Res.	93.9±0.2%	95.5±0.1%
II _A		97.1±0.2%	
I _B	LA	96.6±0.4%	95.2±0.1%
II _B		93.8±0.2%	

TABLE II: Individual two-photon indistinguishability of sources {I_A, II_A} for successively emitted photons (12 ns apart) when paired under resonant excitation, and {I_B, II_B} when paired under LA-phonon-assisted excitation.

V. DISCUSSION

To understand the physical phenomena at the origin of the remaining distinguishability between remote sources, we consider the *individual* two-photon indistinguishability M_i of source i for successively emitted photons [42]. The corresponding values have been measured for the 2 pairs yielding the best *remote* two-photon indistinguishability and are shown in Tab. II for photons emitted 12 ns apart. The measured value above 93.8% indicate a low degree of pure dephasing for each source.

Considering the influence of pure dephasing only, the expected remote mean wavepacket overlap $M_{i,j}$ is given by

$$M_{i,j} = s_{i,j} \frac{(\Gamma_i + \Gamma_j)(\gamma_i + \gamma_j)}{(\Gamma_i + \Gamma_j)^2 + 4\Delta_{i,j}^2}, \quad (5)$$

where $\Gamma_i = \gamma_i + \gamma_i^*$ is the total Lorentzian spectral width (see Supporting Information). With the measured near-unity classical temporal overlap $s_{i,j} \sim 1$, and the high degree of indistinguishability between successively emitted photons, we find an upper bound to

the remote two photon visibility $V_{TPI} = M_{i,j}$ given by $M_{i,j} \leq \min(s_{i,j}, \sqrt{M_i M_j})$ (see Supporting Information). Note that, we can identify here the remote mean wavepacket overlap $M_{i,j}$ with the two-photon indistinguishability V_{TPI} considering the negligible $g^{(2)}(0)$ of the sources. We find that the measured values of remote indistinguishability reported in Tab. I do not reach the upper bounds deduced from individual source indistinguishability, showing that it is not limited by temporal, frequency matching or pure dephasing.

The reduced values of remote indistinguishability is thus mainly limited by $\Delta_{i,j}$ fluctuating over the measurement

$$\langle M_{i,j} \rangle_{\Delta} = \frac{\pi}{2} s_{i,j}^2 (\gamma_i + \gamma_j) V(\bar{\Delta}_{i,j}; \bar{\Gamma}_{i,j}, \delta\omega_{i,j}) \quad (6)$$

where $\bar{\Gamma}_{i,j} = (\Gamma_i + \Gamma_j)/2$ is the average spectral width of the two photons. To test the validity of this analysis, we measure the indistinguishability of different photons emitted by the same source as a function of the time delay between the emitted photons of each source for source I_A and II_A to access the temporal decoherence γ_i^* and the amplitude of the emission energy fluctuation $\delta\omega_i$.

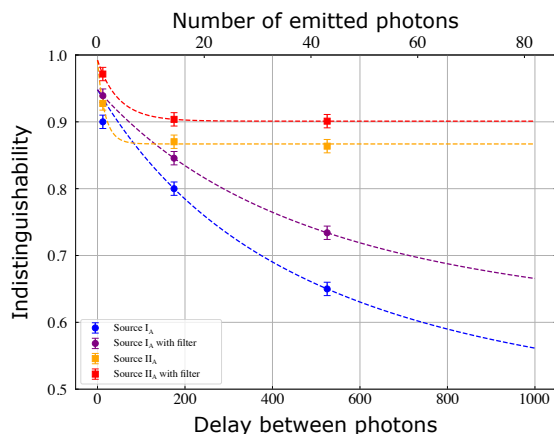


FIG. 5: Indistinguishability of sources I_A and II_A as a function of the delay between the 2 interfering photons for a resonant excitation scheme. The spectral filter improves the visibility of the HOM interferences by filtering part of the phonon sideband, and reducing the spectral wandering of the emission line.

A variable delay is set on a path-unbalanced Mach-Zehnder interferometer to study the indistinguishability of photons separated by an increasing time up to 525 ns. Fig. 5 shows the results obtained for sources I_A and II_A with and without an additional 8 pm width spectral filter. The individual indistinguishability of source I_A decreases from $(89.65 \pm 0.01)\%$ to $(64.6 \pm 0.1)\%$ going from a 12.2 ns

time scale, i.e. the independent spectral wandering of each source. We make the assumption that each source follows independent normal distributions with mean frequency ω_i and standard deviations $\delta\omega_i$ [43]. We define the random variable $\Delta_{i,j}$, also normally distributed, with a mean value $\bar{\Delta}_{i,j} = \omega_i - \omega_j$ and standard deviation $\delta\omega_{i,j} = \sqrt{\delta\omega_i^2 + \delta\omega_j^2}$ and average Eq. (5) [44].

For the specific case of photons with a Lorentzian spectral shape, we can simply average Eq. (5). Note that this is equivalent to taking the convolution of a Lorentzian function with a Gaussian function, and hence the result of the mean wavepacket overlap contains a Voigt function V :

to a 525 ns delay, while for source II_A the indistinguishability decreases from $(92.75 \pm 0.01)\%$ to $(86.36 \pm 0.1)\%$ without spectral filter. With the additional spectral filter, the indistinguishability of source I_A decreases from $(93.9 \pm 0.2)\%$ to $(73.4 \pm 0.2)\%$ going from a 12.2 ns to a 525 ns delay, while for source II_A the indistinguishability decreases from $(97.1 \pm 0.2)\%$ to $(90.1 \pm 0.2)\%$

Considering a near-perfect single photon purity ($g^{(2)}(0) = 0$), the visibility dependence is given by [43]:

$$V(\tau) = \frac{V(\tau = 0)}{1 + 2\delta\omega_r^2(1 - e^{-\Delta\tau/\tau_c})} \quad (7)$$

where $V(\tau = 0) = \gamma/(\gamma + \gamma^*)$ is the "intrinsic" degree of indistinguishability limited by pure dephasing only, τ_c a characteristic wandering timescale, and $\delta\omega_r = \delta\omega/(\gamma + \gamma^*)$ is the ratio between the frequency detuning and the spectral linewidth $\gamma + \gamma^*$.

We fit Eq. (7) on the dataset presented in Fig. 5 to extract a lower bound the spectral amplitude of spectral diffusion for each source [45]. For a single source, we use the same value of indistinguishability $V(0)$ for a zero time delay between photons. For each source, we can then extract the broadening due to pure dephasing and spectral wandering of both sources using Eq. (7) to derive $\gamma_{I_A}^* = (0.17 \pm 0.01) \text{ ns}^{-1}$ and $\gamma_{II_A}^* = (0.03 \pm 0.01) \text{ ns}^{-1}$ and fit $\delta\omega_{I_A} = 4.7 \text{ ns}^{-1}$ ($\delta\omega_{I_A} = 4.6 \text{ ns}^{-1}$), and $\delta\omega_{II_A} = 2.12 \text{ ns}^{-1}$ ($\delta\omega_{II_A} = 1.78 \text{ ns}^{-1}$) without (with) spectral filtering. Using Eq. (6), we derive a limit for M_{I_A, II_A} , yielding $M_{I_A, II_A} < (65 \pm 1)\%$ ($M_{I_A, II_A} < (71 \pm 1)\%$) without (with) spectral filtering, values that are in good agreement with our remote source interference measurements.

We note that the samples under study show increased spectral diffusion compared to other source samples as reported previously in references [43, 46] a difference that could be attributed to a difference in the dopants used in the p-i-n diode.

VI. CONCLUSION

In conclusion, we have reported on record remote indistinguishability for multiple deterministically fabricated quantum dot sources in cavities. Remote indistinguishabilities in the 44-69% range were reported on several pairs of sources. All measurements were taken at maximum occupation probability for each source, i.e. at maximal brightness at mutual source resonance. Our study shows that the reduction of two-photon interference visibility mostly arises from spectral wandering, most probably originating from slow electrical and magnetic noise. More studies will be required to further reduce the influence of these noises. In particular, better understanding could be obtained exploiting well-known noise spectroscopy techniques [47] to identify the influence of the as-grown material structure (doping, p-i-n diode structure), the influence of the cavity processing recipes (etching, annealing) as well as the stability of the control electronics. We finally note that these high values of remote indistinguishability have been obtained both on neutral and charged QDs. The remote interference of such bright

sources embedding a single spin acting as a local quantum bits has recently been shown to be highly beneficial to scale-up optical quantum computing [17, 48, 49]. As such, the present study sets the ground to head toward resource-efficient fault tolerant optical quantum computing.

Note – During the writing of this manuscript, we became aware of the following works [50] and [51] of relevance to the present study.

ACKNOWLEDGMENTS

This work was partly supported the European Union's Horizon 2020 FET OPEN project PHOQUSING (Grant ID 899544), the European Union's Horizon 2020 Research and Innovation Programme QUDOT-TECH under the Marie Skłodowska-Curie Grant Agreement No. 861097, by the Horizon-CL4 program under the grant agreement 101135288 for the EPIQUE project, by the Plan France 2030 through the projects ANR-22-PETQ-0013, the French RENATECH network, the Paris Ile-de-France Region in the framework of DIM SIRTEQ.

-
- [1] H.-S. Zhong, Y. Li, W. Li, L.-C. Peng, Z.-E. Su, Y. Hu, Y.-M. He, X. Ding, W. Zhang, H. Li, *et al.*, *Physical review letters* **121**, 250505 (2018).
- [2] X.-L. Wang, Y.-H. Luo, H.-L. Huang, M.-C. Chen, Z.-E. Su, C. Liu, C. Chen, W. Li, Y.-Q. Fang, X. Jiang, *et al.*, *Physical review letters* **120**, 260502 (2018).
- [3] C. Vigliar, S. Paesani, Y. Ding, J. C. Adcock, J. Wang, S. Morley-Short, D. Bacco, L. K. Oxenløwe, M. G. Thompson, J. G. Rarity, *et al.*, *Nature Physics* **17**, 1137 (2021).
- [4] K. Alexander, A. Bahgat, A. Benyamini, D. Black, D. Bonneau, S. Burgos, B. Burrige, G. Campbell, G. Catalano, A. Ceballos, *et al.*, *arXiv preprint arXiv:2404.17570* (2024).
- [5] P. Senellart, G. Solomon, and A. White, *Nature nanotechnology* **12**, 1026 (2017).
- [6] N. Somaschi, V. Giesz, L. De Santis, J. Loredo, M. P. Almeida, G. Hornecker, S. L. Portalupi, T. Grange, C. Anton, J. Demory, *et al.*, *Nature Photonics* **10**, 340 (2016).
- [7] N. Tomm, A. Javadi, N. O. Antoniadis, D. Najer, M. C. Löbl, A. R. Korsch, R. Schott, S. R. Valentin, A. D. Wieck, A. Ludwig, *et al.*, *Nature Nanotechnology* **16**, 399 (2021).
- [8] R. Uppu, F. T. Pedersen, Y. Wang, C. T. Olesen, C. Papon, X. Zhou, L. Midolo, S. Scholz, A. D. Wieck, A. Ludwig, *et al.*, *Science advances* **6**, eabc8268 (2020).
- [9] H. Wang, J. Qin, X. Ding, M.-C. Chen, S. Chen, X. You, Y.-M. He, X. Jiang, L. You, Z. Wang, *et al.*, *Physical review letters* **123**, 250503 (2019).
- [10] H. Cao, L. Hansen, F. Giorgino, L. Carosini, P. Zakhalka, F. Zilk, J. Loredo, and P. Walther, *arXiv preprint arXiv:2308.05709* (2023).
- [11] L. M. Hansen, L. Carosini, L. Jehle, F. Giorgino, R. Hovenaghel, M. Vyvlecka, J. C. Loredo, and P. Walther, *arXiv preprint arXiv:2304.12956* (2023).
- [12] N. Maring, A. Fyrrillas, M. Pont, E. Ivanov, P. Stepanov, N. Margaria, W. Hease, A. Pishchagin, T. H. Au, S. Boissier, *et al.*, *arXiv preprint arXiv:2306.00874* (2023).
- [13] J.-P. Li, J. Qin, A. Chen, Z.-C. Duan, Y. Yu, Y. Huo, S. Höfling, C.-Y. Lu, K. Chen, and J.-W. Pan, *ACS Photonics* **7**, 1603 (2020).
- [14] J.-P. Li, X. Gu, J. Qin, D. Wu, X. You, H. Wang, C. Schneider, S. Höfling, Y.-H. Huo, C.-Y. Lu, *et al.*, *Physical Review Letters* **126**, 140501 (2021).
- [15] M. Pont, R. Albiero, S. E. Thomas, N. Spagnolo, F. Ceccarelli, G. Corrielli, A. Brieuessel, N. Somaschi, H. Huet, A. Harouri, *et al.*, *arXiv preprint arXiv:2201.13333* (2022).
- [16] M. Pont, G. Corrielli, A. Fyrrillas, I. Agresti, G. Carvacho, N. Maring, P.-E. Emeriau, F. Ceccarelli, R. Albiero, P. H. Ferreira, *et al.*, *arXiv preprint arXiv:2211.15626* (2022).
- [17] S. C. Wein, T. G. de Brugière, L. Music, P. Senellart, B. Bourdoncle, and S. Mansfield, *arXiv preprint arXiv:2412.08611* (2024).
- [18] R. B. Patel, A. J. Bennett, I. Farrer, C. A. Nicoll, D. A. Ritchie, and A. J. Shields, *Nature photonics* **4**, 632 (2010).
- [19] E. B. Flagg, A. Muller, S. V. Polyakov, A. Ling, A. Migdall, and G. S. Solomon, *Physical Review Letters* **104**, 137401 (2010).
- [20] W. Gao, P. Fallahi, E. Togan, A. Delteil, Y. Chin, J. Miguel-Sanchez, and A. Imamoglu, *Nature communications* **4**, 1 (2013).
- [21] Y. He, Y.-M. He, Y.-J. Wei, X. Jiang, M.-C. Chen, F.-L. Xiong, Y. Zhao, C. Schneider, M. Kamp, S. Höfling, *et al.*, *Physical review letters* **111**, 237403 (2013).

- [22] P. Gold, A. Thoma, S. Maier, S. Reitzenstein, C. Schneider, S. Höfling, and M. Kamp, *Physical Review B* **89**, 035313 (2014).
- [23] V. Giesz, S. Portalupi, T. Grange, C. Antón, L. De Santis, J. Demory, N. Somaschi, I. Sagnes, A. Lemaître, L. Lanco, *et al.*, *Physical Review B* **92**, 161302 (2015).
- [24] J.-H. Kim, C. J. Richardson, R. P. Leavitt, and E. Waks, *Nano Letters* **16**, 7061 (2016).
- [25] K. D. Jöns, K. Stensson, M. Reindl, M. Swillo, Y. Huo, V. Zwiller, A. Rastelli, R. Trotta, and G. Björk, *Physical Review B* **96**, 075430 (2017).
- [26] M. Reindl, K. D. Jöns, D. Huber, C. Schimpf, Y. Huo, V. Zwiller, A. Rastelli, and R. Trotta, *Nano letters* **17**, 4090 (2017).
- [27] J. H. Weber, J. Kettler, H. Vural, M. Müller, J. Maisch, M. Jetter, S. L. Portalupi, and P. Michler, *Physical Review B* **97**, 195414 (2018).
- [28] A. Thoma, P. Schnauber, J. Böhm, M. Gschrey, J.-H. Schulze, A. Strittmatter, S. Rodt, T. Heindel, and S. Reitzenstein, *Applied Physics Letters* **110**, 011104 (2017).
- [29] M. Zopf, T. Macha, R. Keil, E. Uruñuela, Y. Chen, W. Alt, L. Ratschbacher, F. Ding, D. Meschede, and O. G. Schmidt, *Physical Review B* **98**, 161302 (2018).
- [30] J. H. Weber, B. Kambs, J. Kettler, S. Kern, J. Maisch, H. Vural, M. Jetter, S. L. Portalupi, C. Becher, and P. Michler, *Nature nanotechnology* **14**, 23 (2019).
- [31] L. Zhai, G. N. Nguyen, C. Spinnler, J. Ritzmann, M. C. Löbl, A. D. Wieck, A. Ludwig, A. Javadi, and R. J. Warburton, *Nature Nanotechnology*, 1 (2022).
- [32] X. You, M.-Y. Zheng, S. Chen, R.-Z. Liu, J. Qin, M.-C. Xu, Z.-X. Ge, T.-H. Chung, Y.-K. Qiao, Y.-F. Jiang, *et al.*, *Advanced Photonics* **4**, 066003 (2022).
- [33] C. Papon, Y. Wang, R. Uppu, S. Scholz, A. D. Wieck, A. Ludwig, P. Lodahl, and L. Midolo, *arXiv preprint arXiv:2210.09826* (2022).
- [34] L. Dusanowski, D. Köck, C. Schneider, and S. Höfling, *arXiv preprint arXiv:2301.01706* (2023).
- [35] A. Dousse, L. Lanco, J. Suffczyński, E. Semenova, A. Mirard, A. Lemaître, I. Sagnes, C. Roblin, J. Bloch, and P. Senellart, *Physical review letters* **101**, 267404 (2008).
- [36] A. Nowak, S. Portalupi, V. Giesz, O. Gazzano, C. Dal Savio, P.-F. Braun, K. Karrai, C. Arnold, L. Lanco, I. Sagnes, *et al.*, *Nature communications* **5**, 1 (2014).
- [37] H. Ollivier, I. M. d. B. Wenniger, S. Thomas, S. Wein, G. Coppola, A. Harouri, P. Hilaire, C. Millet, A. Lemaître, I. Sagnes, O. Krebs, L. Lanco, J. C. Loredo, C. Antón, N. Somaschi, and P. Senellart, *ACS Photonics* **7**, 1050 (2020), *arXiv: 1910.08863*.
- [38] S. Thomas, M. Billard, N. Coste, S. Wein, H. Ollivier, O. Krebs, L. Tazaïrt, A. Harouri, A. Lemaitre, I. Sagnes, *et al.*, *Physical Review Letters* **126**, 233601 (2021).
- [39] X. Ding, Y.-P. Guo, M.-C. Xu, R.-Z. Liu, G.-Y. Zou, J.-Y. Zhao, Z.-X. Ge, Q.-H. Zhang, H.-L. Liu, L.-J. Wang, *et al.*, *arXiv:2311.08347* (2023).
- [40] N. Coste, D. Fioretto, N. Belabas, S. Wein, P. Hilaire, R. Frantzeskakis, M. Gundin, B. Goes, N. Somaschi, M. Morassi, *et al.*, *Nature Photonics* **17**, 582 (2023).
- [41] D. Gammon, E. Snow, B. Shanabrook, D. Katzer, and D. Park, *Physical review letters* **76**, 3005 (1996).
- [42] The single-photon indistinguishability M can be computed from the visibility of the Hong-Ou-Mandel interference fringe V_{HOM} and the $g^{(2)}(0)$ as $M = \frac{V_{HOM} + g^{(2)}(0)}{1 - g^{(2)}(0)}$ [52].
- [43] J. C. Loredo, N. A. Zakaria, N. Somaschi, C. Anton, L. De Santis, V. Giesz, T. Grange, M. A. Broome, O. Gazzano, G. Coppola, *et al.*, *Optica* **3**, 433 (2016).
- [44] Such simplification can be done for lorentzian single photon spectra.
- [45] The datapoint for source I_A without filtering for a delay between photons of $\Delta t = 12$ ns has been treated differently in the numerical fit as it does not allow the fit to converge. We use an error bar of 10% during fit to account for a possible outlier, but display the measure value of 2% in Fig. 5.
- [46] L. De Santis, C. Antón, B. Reznichenko, N. Somaschi, G. Coppola, J. Senellart, C. Gómez, A. Lemaître, I. Sagnes, A. G. White, *et al.*, *Nature nanotechnology* **12**, 663 (2017).
- [47] A. V. Kuhlmann, J. Houel, A. Ludwig, L. Greuter, D. Reuter, A. D. Wieck, M. Poggio, and R. J. Warburton, *Nature Physics* **9**, 570 (2013).
- [48] G. de Gliniasty, P. Hilaire, P.-E. Emeriau, S. C. Wein, A. Salavrakos, and S. Mansfield, *Quantum* **8**, 1423 (2024).
- [49] P. Hilaire, T. Dessertaine, B. Bourdoncle, A. Denys, G. de Gliniasty, G. Valentí-Rojas, and S. Mansfield, *arXiv preprint arXiv:2410.07065* (2024).
- [50] A. Laneve, G. Ronco, M. Beccaceci, P. Barigelli, F. Salusti, N. Claro-Rodriguez, G. De Pascalis, A. Suprano, L. Chiaudano, E. Schöll, *et al.*, *arXiv preprint arXiv:2411.12387* (2024).
- [51] T. Strobel, M. Vyvlecka, I. Neureuther, T. Bauer, M. Schäfer, S. Kazmaier, N. L. Sharma, R. Joos, J. H. Weber, C. Nawrath, *et al.*, *arXiv preprint arXiv:2411.12904* (2024).
- [52] H. Ollivier, S. Thomas, S. Wein, I. M. de Buy Wenniger, N. Coste, J. Loredo, N. Somaschi, A. Harouri, A. Lemaitre, I. Sagnes, *et al.*, *Physical Review Letters* **126**, 063602 (2021).